

Deep Learning Enhanced Dynamic Mode Decomposition

Daniel J. Alford-Lago^{*1,2}, Christopher W. Curtis², Alexander Ihler³,
and Opal Issan⁴

¹*Naval Information Warfare Center Pacific*

²*Department of Mathematics and Statistics, San Diego State University*

³*Department of Computer Science, University of California Irvine*

⁴*Department of Mechanical and Aerospace Engineering, University of California
San Diego*

Abstract

Koopman operator theory shows how nonlinear dynamical systems can be represented as an infinite-dimensional, linear operator acting on a Hilbert space of observables of the system. However, determining the relevant modes and eigenvalues of this infinite-dimensional operator can be difficult. The extended dynamic mode decomposition (EDMD) is one such method for generating approximations to Koopman spectra and modes, but the EDMD method faces its own set of challenges due to the need of user defined observables. To address this issue, we explore the use of autoencoder networks to simultaneously find optimal families of observables which also generate both accurate embeddings of the flow into a space of observables and submersions of the observables back into flow coordinates. This network results in a global transformation of the flow and affords future state prediction via the EDMD and the decoder network. We call this method the deep learning dynamic mode decomposition (DLDMD). The method is tested on canonical nonlinear data sets and is shown to produce results that outperform a standard DMD approach and enable data-driven prediction where the standard DMD fails.

1 Introduction

A central question in applied dynamical systems is one of generating models from measured data so as to facilitate prediction of unmeasured or future states. While the need for such work was clear to researchers several decades ago [1], the ongoing shift occurring in the physical sciences away from first

^{*}daniel.alfordlago@navy.mil

principles modeling to data-driven modeling [2, 3], coupled with the rise in computing power and algorithm design, has added impetus to the search for mathematically robust and generalizable model generating methods.

One particular collection of methods which has garnered significant attention and development are those built around the approximation of Koopman operators, which were first introduced in [4], broadly described as dynamic mode decomposition (DMD) methods. These methods in some sense fit within the larger context of modal decompositions [5, 6], but in several ways, they go further in so far as they also readily generate proxies for the flow maps connected to the otherwise unknown but underlying dynamical systems generating the data in question. The first papers in this area [7, 8] showed across a handful of problems that with a surprisingly straightforward approach, one could readily generate accurate models with nothing but measured time series. Further extensions soon appeared by way of the extended DMD (EDMD) and kernel DMD (KDMD) [9, 10] which generalized the prior approaches in such a way to better exploit the approximation methodologies used in Reproducing Kernel Hilbert Spaces. These methods were used to develop an all purpose approach to model discovery [11]. See [12] for a textbook presentation and summary of what one might describe as the first wave of DMD literature.

However, in the above methods, user choices for how to represent data are necessary, and as shown in [13], even what appear to be natural choices can produce misleading or even outright incorrect results. In response, researchers have brought several supervised learning, or what one might broadly call machine learning (ML), approaches to bear on the problem of finding optimal representations of data for the purpose of approximating Koopman operators. These approaches have included dictionary learning approaches [14, 15] and related kernel learning methods [16]. Likewise, building on theoretical results in [17, 18], more general methods seeking the discovery of optimal topological conjugacies of the flow have been developed [19, 20]. Related work on discovering optimal embeddings of chaotic time series [21], and ML driven model discovery [22] have also recently appeared.

Between these two approaches then, in this work we present a hybrid methodology that explores using ML to discover optimal dictionaries of observables which also effectively ensure that the relevant subspaces in which the dynamics evolves are well approximated. To assess the validity and robustness of our approach, we explore a number of examples motivated by several different planar phase space geometries. We examine how our method deals with the classic nonlinear oscillator, the multiscale Van der Pol oscillator, and the Duffing equation. This presents a range of planar problems in which one has a global center, two centers, and finally a case in which we have slow/fast dynamics on an attractive limit cycle. As we show, our method is able to learn across these different geometries, thereby establishing confidence that it should be adaptable to more complex prob-

lems. Ultimately, we aim to incorporate our method into the larger body of work surrounding surrogate model development in complex flows where optimal bases of representation of the data are critical to the generation of physically realistic simulations.

In Section 2, we introduce the Koopman operator and outline the DMD method for finding a finite dimensional approximation to the Koopman operator. The role of deep autoencoders in our method is presented in Section 3. Results are presented in Section 5. Discussion of results and explorations of future directions are presented in Section 6.

2 The Koopman Operator and Dynamic Mode Decomposition

In this work, we seek to generate approximate predictive models for time series, say $\{\mathbf{y}_j\}_{j=1}^{N_T+1}$, which are generated by an unknown dynamical system of the form

$$\frac{d}{dt}\mathbf{y}(t) = f(\mathbf{y}(t)), \quad \mathbf{y}(0) = \mathbf{x} \in \mathcal{M} \subseteq \mathbb{R}^{N_s}, \quad (1)$$

where \mathcal{M} is some connected, compact subset of \mathbb{R}^{N_s} . We denote the affiliated flow of this equation as $\mathbf{y}(t) = \varphi(t; \mathbf{x})$, and *observables* of the state as $g(\mathbf{y}(t))$, where $g : \mathcal{M} \mapsto \mathbb{C}$. To build these approximate predictive models, we build on the seminal work in [4] which shows that there exists a linear representation of the flow map given by the *Koopman* operator \mathcal{K}^t where

$$\mathcal{K}^t g(\mathbf{x}) = g(\varphi(t; \mathbf{x})). \quad (2)$$

Linearity is gained at the cost of turning the problem of predicting a finite-dimensional flow into one of examining the infinite dimensional structure of the linear operator \mathcal{K}^t . To wit, if we consider the observables g to be members of the associated Hilbert space of *observables*, say $L_2(\mathcal{M}, \mathbb{C})$, $g \in L_2(\mathcal{M}, \mathbb{C})$ if $\|g\|_2 < \infty$ where $\|g\|_2$ is given by

$$\|g\|_2^2 = \int_{\mathcal{M}} |g(\mathbf{x})|^2 d\mathbf{x}.$$

For concreteness, we have chosen to integrate with respect to Lebesgue measure, though of course others could be more convenient or appropriate. We see then that this makes the Koopman operator \mathcal{K}^t an infinite-dimensional map such that

$$\mathcal{K}^t : L_2(\mathcal{M}, \mathbb{C}) \rightarrow L_2(\varphi_{-t}(\mathcal{M}), \mathbb{C}).$$

In this case, one has

$$\begin{aligned} \|\mathcal{K}^t g\|_2^2 &= \int_{\varphi_{-t}(\mathcal{M})} |g(\varphi(t; \mathbf{x}))|^2 d\mathbf{x}, \\ &= \int_{\mathcal{M}} |g(\mathbf{x})|^2 J^{-1}(t; \mathbf{x}) d\mathbf{x}, \\ &\leq \left(\sup_{\mathbf{x} \in \mathcal{M}} J^{-1}(t; \mathbf{x}) \right) \|g\|_2^2, \end{aligned}$$

where

$$J(t; \mathbf{x}) = |\det(D_{\mathbf{x}}\varphi(t; \mathbf{x}))|.$$

Based on the above computations, we observe that the Koopman operator is an isometry for volume preserving flows.

If we further suppose that \mathcal{M} is invariant with respect to the flow, or $\varphi_t(\mathcal{M}) \subset \mathcal{M}$ for $t > 0$, we can simplify the above statement so that

$$\mathcal{K}^t : L_2(\mathcal{M}, \mathbb{C}) \rightarrow L_2(\mathcal{M}, \mathbb{C}).$$

We will assume this requirement going forward since it is necessary to make much in the way of concrete statements about the analytic properties of the Koopman operator. In particular, using Equation (2), if we further suppose that we have an observable g such that $g \in C_1(\mathcal{M})$ then we see that

$$\lim_{t \rightarrow 0^+} \frac{\|\mathcal{K}^t g - g\|_{\infty}}{t} = \|f \cdot \nabla g\|_{\infty},$$

where $\|\cdot\|_{\infty}$ denotes the supremum norm over the compact subset \mathcal{M} . From this computation, we find that the infinitesimal generator, say \mathcal{L} , affiliated with \mathcal{K}^t is given by

$$\mathcal{L}g = f(\mathbf{x}) \cdot \nabla g,$$

and we likewise can use the Koopman operator to solve the initial-value problem

$$u_t = \mathcal{L}u, \quad u(\mathbf{x}, 0) = g(\mathbf{x}),$$

so that $u(\mathbf{x}, t) = \mathcal{K}^t g(\mathbf{x})$. From here, the central question in Koopman analysis is to determine the spectrum and affiliated modes of \mathcal{L} since these then completely determine the behavior of \mathcal{K}^t . This can of course involve solving the classic eigenvalue problem

$$\mathcal{L}\phi = \lambda\phi.$$

However, as the reader may have noticed, there has been no discussion of boundary conditions. So while one can get many useful results focusing on this problem, one must also allow that continuous spectra is a natural

feature, and eigenfunctions can have pathological behavior as well as being difficult to categorize completely and in detail; see [18] and [23]. As this issue represents an evolving research area, we do not attempt to make any further claim and simply follow in the existing trend of the literature and focus on trying to numerically solve the classic eigenvalue problem.

To this end, if we can find the Koopman eigenfunctions $\{\phi_l\}_{l=1}^{\infty}$ with affiliated eigenvalues $\{\lambda_l\}_{l=1}^{\infty}$, where

$$\mathcal{K}^t \phi_l = e^{t\lambda_l} \phi_l, \quad l \in \{1, 2, \dots\},$$

then for any observable g one in principal has a modal decomposition such that

$$g(\mathbf{x}) = \sum_{l=1}^{\infty} c_l \phi_l(\mathbf{x}),$$

as well as an analytic representation of the associated dynamics

$$\mathcal{K}^t g(\mathbf{x}) = \sum_{l=1}^{\infty} c_l e^{t\lambda_l} \phi_l(\mathbf{x}). \quad (3)$$

Note, the analytic details we provide regarding the Koopman operator in this section are those we find most essential to understanding the present work and for providing a reasonably complete reading experience. Essentially all of it exists, and more detail and depth can be found, in [24, 25, 26] among many other sources.

Now, the challenge of determining the modes and eigenvalues of the infinite-dimensional operator, \mathcal{K}^t , remains. In general, this is impossible to obtain in an analytic way, however, the DMD and its extensions, the EDMD and the KDMD [7, 8, 12, 9, 10], allow for the numerical determination of a finite number of the Koopman modes and eigenvalues. In this work, we focus on the EDMD since it most readily aligns with the methodologies of ML.

The EDMD begins with the data set $\{\mathbf{y}_j\}_{j=1}^{N_T+1}$ where

$$\mathbf{y}_j = \varphi(t_j; \mathbf{x}), \quad t_j = (j-1)\delta t,$$

where δt is the time step at which data is sampled. Note, per this definition, we have that $\mathbf{y}_1 = \mathbf{x}$. Following [9, 10], given our time snapshots $\{\mathbf{y}_j\}_{j=1}^{N_T+1}$, we suppose that any observable $g(\mathbf{x})$ of interest lives in a finite-dimensional subspace $\mathcal{F}_D \subset L_2(\mathcal{O})$ described by a given basis of observables $\{\psi_l\}_{l=1}^{N_o}$ so that

$$g(\mathbf{x}) = \sum_{l=1}^{N_o} a_l \psi_l(\mathbf{x}). \quad (4)$$

Given this ansatz, we then suppose that

$$\begin{aligned}\mathcal{K}^{\delta t}g(\mathbf{x}) &= \sum_{l=1}^{N_o} a_l \psi_l(\varphi(\delta t, \mathbf{x})) \\ &= \sum_{l=1}^{N_o} \psi_l(\mathbf{x}) (\mathbf{K}_o^T \mathbf{a})_l + r(\mathbf{x}; \mathbf{K}_o)\end{aligned}\tag{5}$$

where $r(\mathbf{x}; \mathbf{K}_o)$ is the associated error which results from the introduction of the finite-dimensional approximation of the Koopman operator represented by the $N_o \times N_o$ matrix \mathbf{K}_o .

While we ultimately find a matrix \mathbf{K}_o to minimize the error $r(\mathbf{x}; \mathbf{K}_o)$ relative to the choice of observables, for this approach to make any real computational sense, we tacitly make the following assumption when using the EDMD

Ansatz 1. *We have chosen observables $\{\psi_l\}_{l=1}^{N_o}$ such that the space*

$$\mathcal{F}_D = \text{Span}\left(\{\psi_l\}_{l=1}^{N_o}\right)$$

is invariant under the action of the Koopman operator $\mathcal{K}^{\delta t}$, i.e.

$$\mathcal{K}^{\delta t} \mathcal{F}_D \subset \mathcal{F}_D.$$

Equivalently, we suppose there exists a set of observables for which the affiliated error $r(\mathbf{x}; \mathbf{K}_o)$ in Equation (4) is identically zero.

We see that if this condition holds for $\mathcal{K}^{\delta t}$, then it also holds for $\mathcal{K}^{n\delta t}$, where n is an integer such that $n \geq 1$, so this Ansatz is stable with respect to iteration of the discrete time Koopman operator. If this condition does not hold, or at least hold up to some nominal degree of error, then one should not imagine that the EDMD method is going to provide much insight into the behavior of the Koopman operator.

One can then demonstrate, in line with the larger DMD literature, that finding the error minimizing matrix \mathbf{K}_o is equivalent to solving the optimization problem

$$\mathbf{K}_o = \underset{\mathbf{K}}{\operatorname{argmin}} \|\Psi_+ - \mathbf{K}\Psi_-\|_F^2, \tag{6}$$

where the $N_o \times N_T$ matrices Ψ_{\pm} are given by

$$\Psi_- = \{\Psi_1 \ \Psi_2 \ \cdots \ \Psi_{N_T}\}, \quad \Psi_+ = \{\Psi_2 \ \Psi_3 \ \cdots \ \Psi_{N_T+1}\}, \tag{7}$$

where each column in the above matrices is a $N_o \times 1$ vector of observables of the form

$$\Psi_j = (\psi_1(\mathbf{y}_j) \ \cdots \ \psi_{N_o}(\mathbf{y}_j))^T,$$

where $\|\cdot\|_F$ is the Frobenius norm. In practice, we solve (6) using the Singular Value Decomposition (SVD) of Ψ_- so that

$$\Psi_- = \mathbf{U}\Sigma\mathbf{W}^\dagger.$$

This then gives us

$$\mathbf{K}_o = \Psi_+ \mathbf{W}\Sigma^{-P}\mathbf{U}^\dagger,$$

where $-P$ denotes the Moore–Penrose pseudoinverse. The corresponding error in the Frobenius norm $E_r(\mathbf{K}_o)$ is given by

$$E_r(\mathbf{K}_o) = \left\| \Psi_+ \left(\mathbf{I} - \mathbf{W}\mathbf{W}^\dagger \right) \right\|_F.$$

We see that $E_r(\mathbf{K}_o)$ serves as a proxy for the error function $r(\mathbf{x}; \mathbf{K}_o)$.

Following existing methodology [9], if we wished to find Koopman eigenfunctions and eigenvalues, then after diagonalizing \mathbf{K}_o so that

$$\mathbf{K}_o = \mathbf{V}\mathbf{T}\mathbf{V}^{-1}, \quad \mathbf{T}_{ll} = \tilde{t}_l,$$

then one can show that the quantity $\lambda_l = \ln(\tilde{t}_l)/\delta t$ should be an approximation to an actual Koopman eigenvalue and

$$\phi_l(\mathbf{x}) = \sum_{m=1}^{N_o} \psi_m(\mathbf{x}) \mathbf{V}_{lm}^{-1}, \quad l = 1, \dots, N_o. \quad (8)$$

From here, in the traditional EDMD algorithm, one approximates the dynamics via the reconstruction formula

$$\mathbf{y}(t; \mathbf{x}) \approx \sum_{l=1}^{N_o} \mathbf{k}_l e^{t\lambda_l} \phi_l(\mathbf{x}),$$

where the *Koopman modes* $\mathbf{k}_l \in \mathbb{C}^{N_s}$ in principal solve the initial-value problem

$$\mathbf{x} = \sum_{l=1}^{N_o} \mathbf{k}_l \phi_l(\mathbf{x}).$$

In the original coordinates of the chosen observables, using Equation (8) we get the equivalent formula

$$\mathbf{y}(t; \mathbf{x}) \approx \mathbf{K}_m e^{t\Lambda} \mathbf{V}^{-1} \Psi(\mathbf{x}),$$

where \mathbf{K}_m is the $N_s \times N_o$ matrix whose columns are the Koopman modes \mathbf{k}_l and Λ is the $N_o \times N_o$ diagonal matrix with diagonal entries λ_l . In practice, we find the Koopman modes via the fitting formula

$$\mathbf{K}_m = \underset{\mathbf{H}}{\operatorname{argmin}} \sum_{j=1}^{N_T+1} \left\| \mathbf{y}_j - \mathbf{H}\mathbf{V}^{-1} \Psi(\mathbf{y}_j) \right\|_2, \quad (9)$$

where \mathbf{H} is any complex $N_s \times N_o$ matrix and the norm $\|\cdot\|_2$ refers to the standard Euclidean norm. Of course, the appropriateness of this fit is completely contingent on the degree to which Ansatz 1 holds. We address this issue in the next section.

Finally, we note that the standard DMD is given by letting $N_o = N_s$ and $\psi_l(\mathbf{x}) = x_l$. In this case, we have that $\mathbf{K}_m = \mathbf{V}$. Due to its popularity and ease of implementation, we use the DMD for reference in Section 5.

3 The Deep Learning Dynamic Mode Decomposition

The central dilemma when using the EDMD is finding suitable collections of observables relative to the data stream $\{\mathbf{y}_j\}_{j=1}^{N_T+1}$. To accomplish this in an algorithmic way, we suppose that an optimal set of observables can be found using a deep neural network \mathcal{E} where

$$\mathcal{E} : \mathbb{R}^{N_s} \rightarrow \mathbb{R}^{N_o}, \quad \mathcal{E}(\mathbf{x}) = \tilde{\mathbf{x}},$$

and where across dimensions we define

$$\tilde{x}_l = \mathcal{E}_l(\mathbf{x}), \quad l = 1, \dots, N_o.$$

We call this the *encoder* network and the transformed coordinates, $\tilde{\mathbf{x}}$, the *latent variables*. Given that the neural network representing \mathcal{E} consists of almost everywhere smooth transformations, we note that by Sard's Theorem [27], we can generically assume that \mathcal{E} has a Jacobian of full rank at almost all points in the domain of the encoder. We generically assume that the latent dimension $N_o \geq N_s$, making \mathcal{E} an immersion [27] from the flow space into the space of observables. In this case, the matrices Ψ_{\pm} from equation (7) are now given by

$$\Psi_- = \{\tilde{\mathbf{y}}_1 \cdots \tilde{\mathbf{y}}_{N_T}\}, \quad \Psi_+ = \{\tilde{\mathbf{y}}_2 \cdots \tilde{\mathbf{y}}_{N_T+1}\}, \quad \tilde{\mathbf{y}}_j = \mathcal{E}(\mathbf{y}_j),$$

so that we compute \mathbf{K}_o in the latent coordinates. Beyond the lower bound given above, we do not enforce any constraint on the number of dimensions of the latent space. Instead, N_o is treated as a hyperparameter. This is a key feature of our encoder networks as they are allowed to lift the data into higher dimensional latent spaces, giving the EDMD a rich, and flexibly defined, space of observables with which to work.

Corresponding to the immersion \mathcal{E} , we introduce the *decoder* network \mathcal{D} which is meant to act as the inverse of \mathcal{E} , i.e. we seek a decoder mapping acting as a submersion

$$\mathcal{D} : \mathbb{R}^{N_o} \rightarrow \mathbb{R}^{N_s},$$

so that

$$\mathcal{D} \circ \mathcal{E}(\mathbf{x}) = \mathbf{x}. \tag{10}$$

Upon finding such a mapping, we can show the following lemma.

Lemma 1. *If for immersion $\mathcal{E} : \mathbb{R}^{N_s} \rightarrow \mathbb{R}^{N_o}$ there exists corresponding submersion $\mathcal{D} : \mathbb{R}^{N_o} \rightarrow \mathbb{R}^{N_s}$ such that*

$$\mathcal{D} \circ \mathcal{E}(\mathbf{x}) = \mathbf{x},$$

then \mathcal{E} is injective and therefore an embedding.

Proof. Suppose

$$\mathcal{E}(\mathbf{x}_1) = \mathcal{E}(\mathbf{x}_2).$$

Then we see by identity that

$$\mathcal{D} \circ \mathcal{E}(\mathbf{x}_1) = \mathcal{D} \circ \mathcal{E}(\mathbf{x}_2),$$

and therefore $\mathbf{x}_1 = \mathbf{x}_2$. Thus \mathcal{E} is an embedding. \square

As shown in [25, 18], flows which are diffeomorphic to one another share Koopman eigenvalues and have eigenfunctions which are identical up to diffeomorphism. In our case, \mathcal{E} and \mathcal{D} are typically not invertible since the reverse composition, $\mathcal{E} \circ \mathcal{D}$, does not necessarily yield the identity. However, we can define the affiliated flow $\tilde{\varphi}(t; \tilde{\mathbf{x}})$ such that

$$\tilde{\varphi}(t; \tilde{\mathbf{x}}) = \mathcal{E}(\varphi(t; \mathbf{x})).$$

Immediately, we find that there must of course be an affiliated Koopman operator, $\tilde{\mathcal{K}}^t$, corresponding to this encoded, or lifted, flow. This then allows us to show the following theorem.

Theorem 1. *With \mathcal{E} and \mathcal{D} as above, if $(\phi(\mathbf{x}), e^{\lambda t})$ are a spectral pair for the Koopman operator \mathcal{K}^t , then $(\tilde{\phi}(\tilde{\mathbf{x}}), e^{\lambda t})$ are a spectral pair for the Koopman operator $\tilde{\mathcal{K}}^t$ where $\tilde{\phi} = \phi \circ \mathcal{D}$.*

Proof. For the operator \mathcal{K}^t , if we suppose it has eigenfunction $\phi(\mathbf{x})$ with corresponding eigenvalue $e^{\lambda t}$, then we have the identities

$$\mathcal{K}^t \phi(\mathbf{x}) = e^{\lambda t} \phi(\mathbf{x}) = \phi(\varphi(t; \mathbf{x})).$$

We then have the affiliated identities

$$\phi(\varphi(t; \mathbf{x})) = (\phi \circ \mathcal{D})(\tilde{\varphi}(t; \tilde{\mathbf{x}})) = e^{\lambda t} (\phi \circ \mathcal{D})(\tilde{\mathbf{x}}) = \tilde{\mathcal{K}}^t (\phi \circ \mathcal{D})(\tilde{\mathbf{x}}),$$

and so in particular we see that

$$\tilde{\mathcal{K}}^t (\phi \circ \mathcal{D})(\tilde{\mathbf{x}}) = e^{\lambda t} (\phi \circ \mathcal{D})(\tilde{\mathbf{x}}).$$

\square

Thus we see that every Koopman mode and eigenvalue in the original flow space is lifted up by the embedding \mathcal{E} . That said, it is of course possible then that new spectral information affiliated with $\tilde{\mathcal{K}}^t$ can appear, and if we perform the EDMD in the lifted variables, there is no immediate guarantee we are in fact computing spectral information affiliated with the primary Koopman operator \mathcal{K}^t . That said, if in fact Ansatz 1 holds for the given choice of observables, which is to say we have made the right choice of embedding \mathcal{E} , then we can prove the following theorem.

Theorem 2. *Assuming Ansatz 1 holds relative to some choice of observables $\{\psi_l(\mathbf{x})\}_{l=1}^{N_o}$, suppose that the action of $\mathcal{K}^{\delta t}$ on each observable is given by the $N_o \times N_o$ connection matrix $\mathbf{C}(\delta t)$ where*

$$\mathcal{K}^{\delta t} \psi_m(\mathbf{x}) = \sum_{l=1}^{N_o} C_{ml}(\delta t) \psi_l(\mathbf{x}),$$

with C_{ml} denoting the entries of the connection matrix. If $\mathbf{C}(\delta t)$ is diagonalizable, then the EDMD algorithm only computes spectra and eigenfunctions of \mathcal{K}^t , $t > 0$.

Proof. For $g \in \mathcal{F}_D$, we have that

$$g(\mathbf{x}) = \sum_{l=1}^{N_o} a_l \psi_l(\mathbf{x}),$$

If Ansatz 1 holds, it is then the case that

$$\mathcal{K}^{\delta t} \left(\sum_{l=1}^{N_o} a_l \psi_l(\mathbf{x}) \right) = \sum_{m=1}^{N_o} b_m \psi_m(\mathbf{x}),$$

and likewise we must have that

$$\begin{aligned} \mathcal{K}^{\delta t} \left(\sum_{l=1}^{N_o} a_l \psi_l(\mathbf{x}) \right) &= \sum_{l=1}^{N_o} a_l \mathcal{K}^{\delta t} \psi_l(\mathbf{x}) \\ &= \sum_{l=1}^{N_o} \sum_{m=1}^{N_o} a_l C_{lm}(\delta t) \psi_m(\mathbf{x}). \end{aligned}$$

Thus, the action of the Koopman operator is now recast in terms of the following matrix problem

$$\mathbf{C}^T(\delta t) \mathbf{a} = \mathbf{b}.$$

Likewise, if we ask for the corresponding connection matrix of higher powers of $\mathcal{K}^{\delta t}$ so that for integer $n \geq 1$ we have

$$\mathcal{K}^{n\delta t} \left(\sum_{l=1}^{N_o} a_l \psi_l(\mathbf{x}) \right) = \sum_{l=1}^{N_o} \sum_{m=1}^{N_o} a_l C_{lm}(n\delta t) \psi_m(\mathbf{x}).$$

Then we see that

$$\mathbf{C}(n\delta t) = \mathbf{C}(\delta t) \mathbf{C}((n-1)\delta t) ,$$

or, defining $\mathbf{C}(0) = \mathbf{I}$ with \mathbf{I} the $N_o \times N_o$ identity matrix,

$$\mathbf{C}(n\delta t) = \mathbf{C}^n(\delta t) .$$

Moreover, referring to the EDMD algorithm, clearly $\mathbf{C}(\delta t) = \mathbf{K}_o$, so that if $\mathbf{K}_o = \mathbf{V}\mathbf{T}\mathbf{V}^{-1}$, then

$$\mathbf{C}(n\delta t) = \mathbf{V}\mathbf{T}^n\mathbf{V}^{-1} .$$

Choosing then the vector of coefficients \mathbf{a} to be the j^{th} column of $(\mathbf{V}^{-1})^T$ or $\mathbf{a} = (\mathbf{V}^{-1})_j^T$, we see

$$\mathcal{K}^{\delta t} \left(\sum_{l=1}^{N_o} a_l \psi_l(\mathbf{x}) \right) = e^{\delta t \lambda_j} \left(\sum_{l=1}^{N_o} a_l \psi_l(\mathbf{x}) \right) ,$$

so that we have using the EDMD algorithm we see we have computed N_o eigenvalues and eigenvectors of $\mathcal{K}^{\delta t}$. Passing to the infinitesimal generator \mathcal{L} allows us to then extend the result for the Koopman operator \mathcal{K}^t for $t > 0$. \square

So we see on the one hand that the EDMD left to its own devices is prone to introducing perhaps spurious spectral information, and of course, without recourse to a known reference, we have no way in advance of knowing how to tell which results generated via the EDMD produce relevant spectra. We note that this issue was numerically illustrated in [13]. On the other hand, if we can somehow ensure Ansatz 1 holds, then the EDMD is guaranteed to produce meaningful results with essentially zero error. Of course, what remains in either case is the fundamental dilemma of how to choose observables such that Ansatz 1 is enforced, or at least such that the error is guaranteed to be controlled in some uniform way.

To address this dilemma then, we propose the deep learning dynamic mode decomposition (DLDMD), in which we determine the encoder/decoder pair \mathcal{E} and \mathcal{D} by minimizing the following loss function \mathcal{L} , where

$$\mathcal{L} = \alpha_1 \mathcal{L}_{\text{recon}} + \alpha_2 \mathcal{L}_{\text{dmd}} + \alpha_3 \mathcal{L}_{\text{pred}} + \alpha_4 \|\mathbf{W}_g\|_2^2 , \quad (11)$$

such that

$$\mathcal{L}_{\text{recon}} = \frac{1}{N_T + 1} \sum_{j=1}^{N_T+1} \|\mathbf{y}_j - \mathcal{D}(\mathcal{E}(\mathbf{y}_j))\|_2 ,$$

$$\mathcal{L}_{\text{dmd}} = E_r(\mathbf{K}_o) ,$$

$$\mathcal{L}_{\text{pred}} = \frac{1}{N_T} \sum_{j=1}^{N_T} \|\mathbf{y}_{j+1} - \mathcal{D}(\mathbf{V}\mathbf{T}^j\mathbf{V}^{-1}\mathcal{E}(\mathbf{x}))\|_2 ,$$

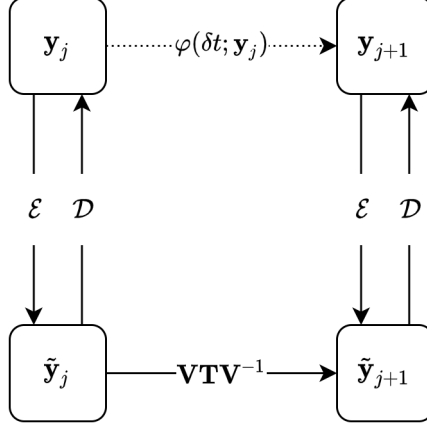


Figure 1: Diagram illustrating the relationships between the encoder (\mathcal{E}), decoder (\mathcal{D}), and DMD ($\mathbf{V}\mathbf{T}\mathbf{V}^{-1}$) steps. Assuming Ansatz 1 holds, these relations are exact. In practice, these are approximations and so we must view the mappings with solid lines as having some affiliated error in a process that allows us to circumvent the unknown flow map $\varphi(\delta t; \mathbf{y}_j)$.

and \mathbf{W}_g contains the weights of the \mathcal{E} and \mathcal{D} networks making the final term in \mathcal{L} a regularization term. The hyperparameters $\alpha_1, \alpha_2, \alpha_3$, and α_4 provide appropriate scalings for each loss component. The autoencoder reconstruction loss, $\mathcal{L}_{\text{recon}}$, demands that \mathcal{D} approximates the inverse of \mathcal{E} . We see then that $\mathcal{L}_{\text{recon}}$ in effect replaces Equation (9). The DMD loss, \mathcal{L}_{dmd} , keeps $r(\mathbf{x}; \mathbf{K}_o)$ as small as possible relative to advancing one timestep. In contrast, we see $\mathcal{L}_{\text{pred}}$ makes the overall method remain stable under repeated applications of the finite dimensional approximation to $\mathcal{K}^{\delta t}$. Thus \mathcal{L}_{dmd} plays the role of ensuring we have a consistent time-stepping scheme, while $\mathcal{L}_{\text{pred}}$ ensures we have a globally stable method, and thereby by combining the two, we address the fundamental dilemma presented by Ansatz 1.

We further see that this loss function implements the diagram in Figure 1. Through this diagram we impose a one-to-one mapping between trajectories in the original coordinates, \mathbf{y} , and trajectories in the latent space, $\tilde{\mathbf{y}}$. Note that this diagram allows us to circumvent the unknown flow map, $\varphi(\delta t; \mathbf{y}_j)$, which is equivalent to the Koopman operator of interest, $\mathcal{K}^{\delta t}$, from Equations (4) and (5).

4 The DLDMD Algorithm: Implementation Details

We build the autoencoder in the Python programming language using Tensorflow version 2. The deep neural networks we construct that act as \mathcal{E}

and \mathcal{D} from Equation (10) must transform each vector of coordinates along a sample trajectory to and from the latent coordinates, respectively. We chose to use dense layers in each network, though other layer types should suffice so long as they encode each point along the trajectory separately, are densely connected, and output the correct dimensions.

As is the case when training any type of neural network, there are a number of hyperparameters that the researcher must take care in selecting. However, we found that the encoder and decoder networks did not require significantly different hyperparameters from dataset to dataset. Throughout all cases, the primary tunable parameter was the dimension of the latent space, N_o . We found that 2 hidden layers each with 128 neurons was sufficient for all of the test problems presented in Section 5. We used Rectified Linear Units (ReLU) for the activation functions and chose the Adam optimizer with a learning rate of 10^{-3} . The loss function hyperparameters in Equation (11), α_1, α_2 , and α_3 were all set to 1, while $\alpha_4 = 10^{-14}$. All models reported in Section 5 were trained using a batch size of 256 for 1,000 epochs. The hardware used was an Nvidia Tesla V100.

See Algorithm 1 for the complete pseudocode for the DLDMD training method. The trained DLDMD model is applied by sending a trajectory through the encoder network, performing the EDMD using the encoded coordinates as observables, then using the modes, eigenvalues, and eigenfunctions to reconstruct the full length of the trajectory and beyond in the latent space. The decoder network then allows us to map the entire EDMD reconstruction back into the original coordinate system.

5 Results

We test the DLDMD method on several planar datasets, each exhibiting its own unique nonlinear dynamical properties. For each dataset we compare reconstructions of the trajectories using the standard DMD in the original phase space against reconstructions from the DLDMD.

The data for each example presented were generated using a fourth-order Runge-Kutta scheme. For the harmonic oscillator, Section 5.1, $\delta t = 0.02$ and $t_f = 6$. The Duffing system used $\delta t = 0.05$ and $t_f = 20$ in order to get multiple periods for each of the closed orbits. Finally, the Van der Pol system used $\delta t = 0.02$ and $t_f = 20$. This system required a shorter integration step size to sufficiently sample the slow and fast parts of each trajectory. It likewise needed longer overall trajectories to ensure that all of the initial conditions ended up near the limit cycle. We generate 15,000 trajectories for each system, using 10,000 for training, 3,000 for validation, and 2,000 for testing. Each trajectory is generated by uniform random sampling of initial conditions from some pre-defined region of phase space. For the harmonic oscillator, we used $x_1 \in \{-3.1, 3.1\}$, $x_2 \in \{-2, 2\}$, and we limited our choice

Algorithm 1: DLDMD

Data: $\mathbf{Y} \in \mathbb{R}^{n \times m}$ such that each column, $\mathbf{y}_i \in \mathbb{R}^n$, is an observation of the state variables δt time from \mathbf{y}_{i-1} .

Result: $\mathcal{E}, \mathcal{D}, \mathbf{T}, \mathbf{V}, \mathbf{k}$

Initialize: set reconstruction weight $\alpha_1 > 0$, DMD prediction weight $\alpha_2 > 0$, phase space prediction weight $\alpha_3 > 0$, and regularization weight $\alpha_4 > 0$.

begin

for $epoch = 1 \dots maxEpochs$ **do**

$\bar{\Psi} \leftarrow \mathcal{E}(\mathbf{Y})$

$\bar{\mathbf{Y}} \leftarrow \mathcal{D}(\bar{\Psi})$

$\Psi_- \leftarrow [\psi_1 \ \psi_2 \ \dots \ \psi_{m-1}]$

$\Psi_+ \leftarrow [\psi_2 \ \psi_3 \ \dots \ \psi_m]$

$\mathbf{U}, \Sigma, \mathbf{W}^\dagger \leftarrow \text{SVD}(\Psi_-)$

$\mathbf{K} \leftarrow \Psi_+ \mathbf{W} \Sigma^{-1} \mathbf{U}^\dagger$

$\mathbf{T}, \mathbf{V} \leftarrow \text{EVD}(\mathbf{K})$

$\mathbf{k} \leftarrow \text{IVP}(\mathbf{V}, \Psi_-)$

for $i = 1 \dots m$ **do**

$\hat{\psi}_i \leftarrow \mathbf{V} \Sigma^i \mathbf{k}$

$\hat{\Psi} \leftarrow [\hat{\psi}_1 \ \hat{\psi}_2 \ \dots \ \hat{\psi}_m]$

$\hat{\mathbf{Y}} \leftarrow \mathcal{D}(\hat{\Psi})$

$\mathcal{L} \leftarrow \alpha_1 \|\bar{\mathbf{Y}} - \mathbf{Y}\|_{\text{MSE}} + \alpha_2 \|\Psi_+(\mathbf{I} - \mathbf{W} \mathbf{W}^\dagger)\|_F$
 $+ \alpha_3 \|\hat{\mathbf{Y}} - \mathbf{Y}\|_{\text{MSE}} + \alpha_4 \|\mathbf{W}_g\|_2^2$

$\mathcal{E}, \mathcal{D} \leftarrow \text{OPT}(\mathcal{L})$

Where $\text{SVD}(\cdot)$ is the Singular Value Decomposition, $\text{EVD}(\cdot)$ is the eigenvalue decomposition, $\text{IVP}(\cdot, \cdot)$ solves an initial value problem, and $\text{OPT}(\cdot)$ is an appropriate optimizer for the neural networks \mathcal{E} and \mathcal{D} . MSE indicates the mean squared error.

of trajectories to those within the first separatrix using the potential function $0.5x_2^2 - \cos x_1 < 0.99$. The Duffing system data was generated over initial conditions sampled from $x_1 \in \{-1, 1\}$ and $x_2 \in \{-1, 1\}$. The Van der Pol system used $x_1 \in \{-2, 2\}$ and $x_2 \in \{-2, 2\}$ to generate trajectories and was then normalized.

5.1 The Harmonic Oscillator: One Center

The first system we consider is a nonlinear oscillator described by the undamped pendulum system,

$$\begin{aligned}\dot{x}_1 &= x_2, \\ \dot{x}_2 &= -\sin(x_1).\end{aligned}$$

This system exhibits nearly linear dynamics in the small angle regime near the origin and becomes increasingly nonlinear near the separatrix. We limited the dataset to just those trajectories that lie below the separatrix in order to test the DLDMD on a system with only closed Hamiltonian orbits about a single center.

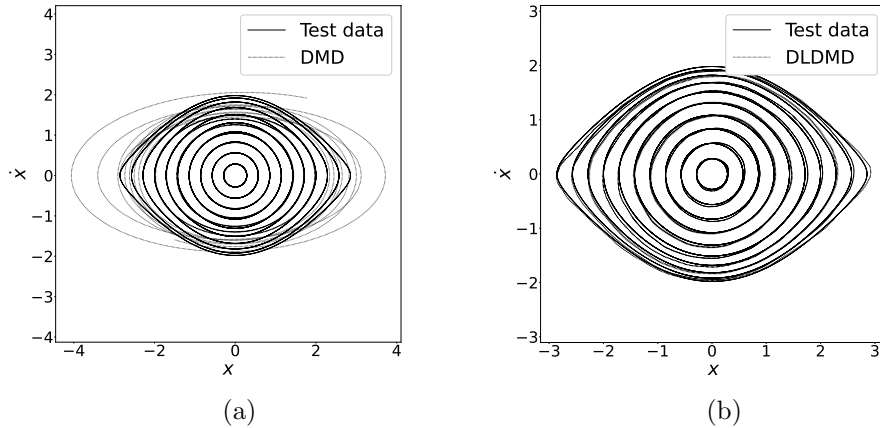


Figure 2: (a) Results from the standard DMD as applied to a harmonic oscillator with the test trajectories (solid lines) and the predicted trajectories from the DMD (dotted lines). (b) Results from the DLDMD as applied to a harmonic oscillator with test trajectories (solid lines) and predicted trajectories from the DLDMD (dotted lines).

Figure 2 shows how the standard DMD approach is only able to reconstruct the oscillations near the linear regime corresponding to small angle displacements. As the angular displacement of the pendulum increases, the DMD’s ability to determine the continuously changing frequency of the pendulum as it begins to stall near the upright position is severely degraded. Conversely, the DLDMD has found a mapping to and from these coordinates

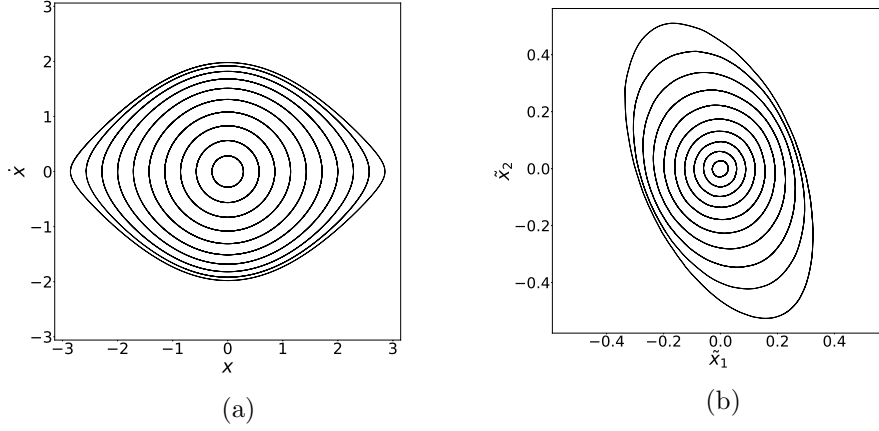


Figure 3: (a) Test trajectories from the harmonic oscillator in the original phase space coordinates. (b) Test trajectories from the harmonic oscillator in the latent space coordinates. These are the trajectories on which the EDMD is applied.

in which it can apply the EDMD with much greater precision and stability. For this example, we found that a latent dimension of $N_o = N_s = 2$ produced the best results. Figure 3 illustrates how the DLDMD has used the encoder network to morph the original test trajectories into a set of coordinates that have less nonlinearity for the DMD to overcome, especially near the separatrix.

5.2 The Duffing Equation: Two Centers

The Duffing system is another weakly nonlinear oscillator with slightly more complex behavior than the undamped pendulum. Without a driving force, the Duffing system is described by the double-well potential Hamiltonian system,

$$\begin{aligned}\dot{x}_1 &= x_2, \\ \dot{x}_2 &= x_1 - x_1^3.\end{aligned}$$

Here we are testing whether the DLDMD can cope with closed orbits that are not all oriented about a single center. Figure 4 shows the enhanced reconstruction capability of the DLDMD over the standard DMD. For this system we found that a latent dimension of $N_o = 3$ produced the best results. Figure 5 shows how the encoder network morphs the trajectories in the original phase space coordinates into paths in the latent space that have a much simpler representation, with each path tracing out nearly circular orbits on this higher dimensional manifold.

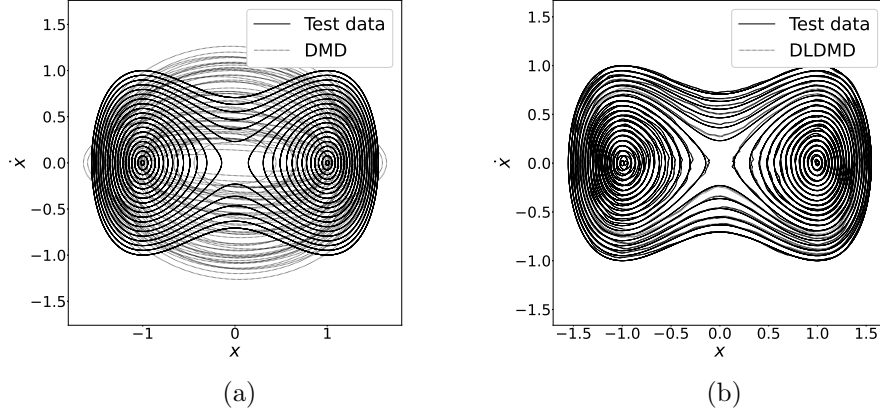


Figure 4: (a) Results from the standard DMD as applied to an unforced Duffing system. The test trajectories (solid lines) and the predicted values from the DMD (dotted lines) show paths in the phase space. (b) Results from the DLDMD as applied to the unforced Duffing system with test trajectories (solid lines) versus predicted values from the DLDMD (dotted lines) in phase space.

5.3 The Van der Pol Oscillator: Attraction to a Slow/Fast Limit Cycle

The Van der Pol oscillator, described by the parametrized dynamical system

$$\begin{aligned}\dot{x}_1 &= x_2, \\ \dot{x}_2 &= \mu(1 - x_1^2)x_2 - x_1,\end{aligned}$$

has for positive values of μ a globally attractive limit cycle. The limit cycle itself is made up of slow and fast submanifolds thereby producing multiscale behavior in the solutions to the Van der Pol equation. This system pushes the DLDMD much further than the harmonic and Duffing oscillators, for it must now account for the attraction onto the limit cycle as well as the periodic motion. Because of the complexity of the nonlinearity present in these trajectories, we found that the DLDMD performed best with $N_o = 8$. The Van der pol system presented here uses the parameter $\mu = 1.5$, however, the DLDMD has been tested out to $\mu = 4$ with no modifications to the algorithm or hyperparameters.

Figure 6 shows the DLDMD predicting the Van der Pol system for several test trajectories while the standard DMD fails to find a sufficient modal decomposition given the restrictive dimensionality of the system.

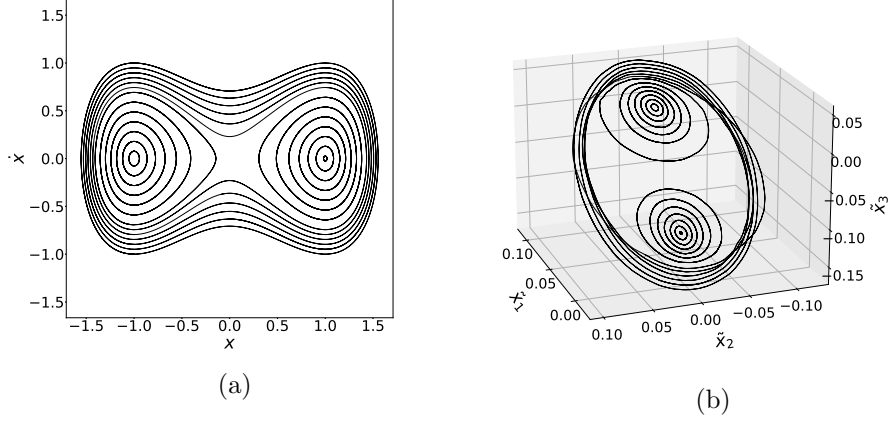


Figure 5: (a) Test trajectories from the unforced Duffing oscillator in the original phase space coordinates. (b) Test trajectories for the Duffing system in the latent space coordinates. These are the trajectories on which the EDMD is applied.

6 Conclusions and Future Directions

This work has shown how flexibility and accuracy can be added to the EDMD by using deep neural network based autoencoders to find optimal latent space coordinates. The DLDMD is shown to enable data-driven prediction on several nonlinear systems for which the standard DMD fails. By constructing a loss function to train the autoencoder using the diagram in Figure 1, we carefully choose mappings to and from the latent space such that the system is one-to-one. Thus we ensure that all Koopman modes and eigenvalues are captured in this latent space as well. However, by lifting into higher dimensional latent spaces we lose the strict topological equivalence in [18] and cannot guarantee all spectra are invariant. Nonetheless, this lifts the burden of choosing the right dictionary for the observables. These dictionaries have historically been comprised of polynomials, Fourier modes, radial basis functions, or spectral elements [9], whereas the autoencoders presented can explore a much more diverse set of dictionary functions that may span the space of observables needed to obtain a proper estimate of the Koopman operator. The \mathcal{L}_{dmd} component of the loss function makes certain that we have a consistent linear fit from one time step to the next, for all observations. Additionally, $\mathcal{L}_{\text{pred}}$ requires that the dynamics of such a fit are stable over time. The combination of these loss terms ensures we come close to satisfying Ansatz 1.

The DLDMD is shown to enhance the reconstruction accuracy of the DMD for several nonlinear dynamical systems, including systems with closed orbits, multiple wells, and attraction onto a limit cycle. Because of the

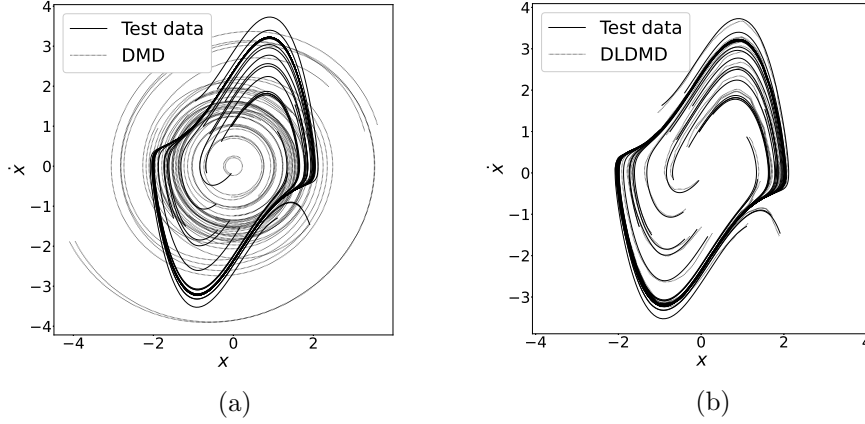


Figure 6: (a) Results from the standard DMD as applied to the Van der Pol system with $\mu = 1.5$. Test trajectories (solid lines) and the predicted values from the DMD (dotted lines) show paths in the phase space. (b) Results from the DLDMD as applied to the Van der Pol oscillator with test trajectories (solid lines) and the predicted values from the DLDMD (dotted lines) in phase space.

impressive flexibility of the autoencoder network, the dimensionality of the latent space was the only hyperparameter that required tuning when training the model on the different datasets. This may be due to the relatively low dimension of these planar systems, making the training process rather insensitive to the number of neurons and layers in the networks. This will likely not be the case for much higher dimensional systems or systems with chaotic or noisy trajectories. In this regard, the method would seem to benefit from some of the alternative views of the standard DMD approach [28, 29], an issue we will pursue in future work.

Data Availability

The data and code that support the findings of this study are openly available at <https://github.com/JayLago/DLDMD.git>

Acknowledgements

This work was supported in part by the Naval Information Warfare Center Pacific (NIWC Pacific) and the Office of Naval Research (ONR).

The authors would like to thank Dr. Erik M. Bollt from the Department of Electrical and Computer Engineering at Clarkson University for his feedback and insights, as well as Joseph Diaz and Robert Simpson for their insightful comments.

References

- [1] H.D.I. Abarbanel, R. Brown, J.J. Sidorowich, and L. Sh. Tsimring. The analysis of observed chaotic data in physical systems. *Rev. Mod. Phys.*, 65:1331–1392, 1993.
- [2] S.L. Brunton, B. R. Noack, and P. Koumoutsakos. Machine learning for fluid mechanics. *Ann. Rev. Fluid Mech.*, 52:477–508, 2020.
- [3] E. Camporeale. The challenge of machine learning in space weather: Nowcasting and forecasting. *Space Weather*, 17:1166–1207, 2019.
- [4] B.O. Koopman. Hamiltonian systems and transformation in Hilbert space. *Proc. Nat. Acad. Sci.*, 17:315–318, 1931.
- [5] P. Benner, S. Gugercin, and K. Willcox. A survey of projection-based model reduction methods for parametric dynamical systems. *SIAM Review*, 57:483–531, 2015.
- [6] K. Taira, S.L. Brunton, S.T.M. Dawson, C.W. Rowley, T. Colonius, B.J. McKeon, O.T. Schmidt, S. Gordeyev, V. Theofilis, and L.S. Ukeiley. Modal analysis of fluid flows: An overview. *AIAA*, 55:4013–4041, 2017.
- [7] P. Schmid. Dynamic mode decomposition of numerical and experimental data. *J. Fluid Mech.*, 656:5–28, 2010.
- [8] I. Mezić. Spectral properties of dynamical systems, model reduction, and decompositions. *Nonlinear Dyn.*, 41:309–325, 2005.
- [9] M.O. Williams, I. G. Kevrekidis, and C. W. Rowley. A data-driven approximation of the Koopman operator: extending dynamic mode decomposition. *J. Nonlin. Sci.*, 25:1307–1346, 2015.
- [10] M.O. Williams, C. W. Rowley, and I. G. Kevrekidis. A kernel-based method for data driven Koopman spectral analysis. *J. Comp. Dyn.*, 2:247–265, 2015.
- [11] S.L. Brunton, J.L. Proctor, and J.N. Kutz. Discovering governing equations from data by sparse identification of nonlinear dynamical systems. *PNAS*, 113:3932–3937, 2016.
- [12] J.N. Kutz, S.L. Brunton, B.W. Brunton, and J.L. Proctor. *Dynamic Mode Decomposition: Data-driven modeling of complex systems*. SIAM, Philadelphia, PA, 2016.
- [13] J.N. Kutz, J.L. Proctor, and S.L. Brunton. Applied Koopman theory for partial differential equations and data-driven modeling of spatio-temporal systems. *Complexity*, 2018:1–16, 2018.

- [14] Q. Li, F. Dietrich, E. Bollt, and I. Kevrekidis. Extended dynamic mode decomposition with dictionary learning: A data-driven adaptive spectral decomposition of the Koopman operator. *Chaos*, 27:103111, 2017.
- [15] E. Yeung, S. Kundu, and N.O. Hodos. Learning deep neural network representations for Koopman operators of nonlinear dynamical systems. In *American Control Conference*, 2019.
- [16] A. M. Degenarro and N. M. Urban. Scalable extended dynamic-mode decomposition using random kernel approximation. *SIAM J. Sci. Comp.*, 41:1482–1499, 2019.
- [17] M. Budisić, R. Mohr, and I. Mezić. Applied koopmanism. *Chaos*, 22(047510), 2012.
- [18] E. Bollt, Q. Li, F. Dietrich, and I. Kevrekidis. On matching, and even rectifying, dynamical systems through koopman operator eigenfunctions. *SIAM J. Appl. Dyn. Sys.*, 17.2:1925–1960, 2018.
- [19] B. Lusch, J. N. Kutz, and S. L. Brunton. Deep learning for universal linear embeddings of nonlinear dynamics. *Nature Comm.*, 9:4950, 2018.
- [20] Jason J. Bramburger, Steven L. Brunton, and J. Nathan Kutz. Deep learning of conjugate mappings. *arXiv*, 2104.01874, 2021.
- [21] W. Gilpin. Deep reconstruction of strange attractors from time series. In *34th Conference on NeurIPS*, 2020.
- [22] K. Champion, B. Lusch, J. N. Kutz, and S. L. Brunton. Data-driven discovery of coordinates and governing equations. *PNAS*, 116:22445–22451, 2019.
- [23] I. Mezić. Spectrum of the koopman operator, spectral expansions in functional spaces, and state-space geometry. *Journal of Nonlinear Science*, 30.5:2091–145, 2019.
- [24] A. Lasota and M. C. Mackey. *Chaos, Fractals, and Noise*. Springer, New York, NY, 2nd edition, 1994.
- [25] M. Budivsić, R. Mohr, and I. Mezić. Applied koopmanism. *chaos*, 22:047510, 2012.
- [26] Efrain Gonzalez, Moad Abudia, Michael Jury, Rushikesh Kamalapurkar, and Joel A. Rosenfeld. Anti-koopmanism, 2021.
- [27] R. Abraham, J.E. Marsden, and T. Ratiu. *Manifolds, Tensor Analysis, and Applications*. Springer, New York, NY, 2nd edition, 2001.

- [28] H. Arbabi and I. Mezić. Ergodic theory, dynamic mode decomposition, and computation of spectral properties of the koopman operator. *SIAM Journal on Applied Dynamical Systems*, 16:2096–2126, 2017.
- [29] S. L. Brunton, B. W. Brunton, J. L. Proctor, E. Kaiser, and J. N. Kutz. Chaos as an intermittently forced system. *Nature Comm.*, 8(1), 2017.